

Conceptual Design of a Variable Stiffness Mechanism in a Humanoid Ankle using Parallel Redundant Actuation

Christoph Stoeffler¹, Shivesh Kumar¹, Heiner Peters¹, Olivier Brüls², Andreas Müller³ and Frank Kirchner¹

Abstract—Future robots will rely more than today on high precision, better energy efficiency and safe handling (e.g. human-machine interaction). An inevitable step in the development of new robots is therefore the improvement of existing mechanisms, since better sensors and algorithms do not satisfy the demands alone. During the last three decades, Parallel Redundant Mechanisms (PRM) came more into the focus of research, as they are advantageous in terms of singularity avoidance, fast movements and energy efficiency. Subsequently, yet another technology - the Variable Impedance Actuator (VIA) - emerged which proposes to change its inherent stiffness allowing an adaptation to its environment and to handle for example dynamic movements or shock absorptions. This work aims to create a new mechanism where a stiffness and position control for 2 degrees of freedom (DOF) is achieved by 3 actuators with flexible elements. It is thus a combination of the PRM and VIA, while taking advantage of both technologies but asking for a more sophisticated mathematical description. Practical implementation is intended for a humanoid ankle mechanism. Kinetostatic and stiffness models are derived and incorporated into the simulation of the mechanism. The simulations show that improvements in terms of singularity removal and dexterity are achieved. Furthermore, the adaptation of human like gait performances is presented.

I. INTRODUCTION

A challenge in present mechanical designs for humanoid robots is the speed and force limitations of its joints. This is mainly due to the structure of the robots limbs that are often arranged in serial arrangement, where the actuators are directly integrated in the joint. The placement of motors and drives in the limb joints results in a serial mechanism (SM) which is a space saving design method, but often restricts the reachable velocities and forces in the *work space* directly to the performance of the actuators. In contrast, *parallel mechanisms* (PMs) consist of closed-loop kinematic chains, which allows one to place the actuators arbitrarily in those chains to drive the mechanism's degrees of freedom (DOF). Compared to SMs, they have a higher structural stiffness, allow better positioning and can be better adapted to movements and forces in the work space because of their linkages. Also, the actuators can be placed more advantageously in the mechanism what reduces the masses of moving parts and allows one to achieve movements with

high dynamics. Those reasons make e.g. the Delta-robot a remarkable representative of PMs (see [23]). In the context of humanoid robotics and exoskeletons, PMs have been used as a mechanical generator of certain kinematic joints such as in torso, wrist, hip and ankle [14, 15, 18, 24]. PMs possess different types of singularities as described in [7]. A possibility of singularity removal lies in an over-actuation of the mechanisms DOF and such systems are then called *parallel-redundant mechanisms* (PRMs). Redundancy here refers to kinematic and actuation redundancy what is e.g. discussed by [19] and brings also advantages in terms of workspace enlargement, improved joint-torque distribution and the possibility of active stiffness control - by antagonistic actuation - as shown by [4, 26].

Soft robotics and increased locomotive performances is becoming increasingly relevant for current and future humanoid robots. During the last decades a continuous improvement in computational performance was achieved which led to development of sophisticated control possibilities and allowed e.g. to achieve compliant behaviour, as shown by [6, 25] and more recently by [5]. Compliant behaviour is usually achieved in the robot's control loop. However, a key ability to reach human (or animal) like performances is to store and release energy within the locomotion. Moreover, the absorption of shocks and safe environmental interaction can be easier achieved by intrinsically compliant design. A common belief is thus that intrinsically compliant designs will drive the future development of robotics, as expressed by [8] and [22]. A mechanical approach for compliant actuators is the *series-elastic actuator* that is widely applied in humanoid designs, exoskeletons and prosthesis [12]. For a direct stiffness control of one DOF, the *Variable Impedance Actuator* (VIA) was first proposed by [10] and is assessed e.g. by [28, 29]. A general overview of the state of the art in soft robotics and VIAs can be found in [3] and [2]. The necessity of introducing non-linearity in the mechanism to achieve stiffness modulation is demonstrated for VIAs in [9].

Motivation: VIAs allow for independent position and stiffness control of one DOF joints by using two actuators. Following the trend of highly integrated multi-DOF joints in robotics (see [14, 15, 18, 24]), it will be desirable to have multi-DOF variable impedance joints. However, utilizing two actuators per joint in a serial architecture may significantly increase the weight of the robot and reduce its dynamic performance. Hence, it is desirable to develop

¹ German Research Center for Artificial Intelligence GmbH - Robotics Innovation Center (DFKI Bremen), Robert-Hooke Str. 1, 28359 Bremen, GERMANY {christoph.stoeffler, shivesh.kumar, heiner.peters, frank.kirchner}@dfki.de

²University of Liège - Department of Aerospace and Mechanical Engineering, Allée de la Découverte 9 (B52/3), B-4000 Liège, BELGIUM o.bruls@uliege.be

³Institute of Robotics, Johannes Kepler University, Linz 4040, AUSTRIA a.mueller@jku.de

parallel mechanisms with similar properties as VIAs. An immediate advantage of such a design is its capability to store and release energy in the elastic elements. We introduce the definition of the *variable stiffness mechanism* (VSM):

A variable stiffness mechanism is any parallel mechanism which allows independent control of end-effector's position and stiffness simultaneously.

Hypothesis: We hypothesize that a VSM can be achieved by utilizing a PM that is added by at least one additional actuator in parallel, while all actuators are complemented by non-linear springs in series. Such a mechanism would allow an independent control of the end-effector position and some stiffness components. This paper addresses specific application for a humanoid ankle design and puts the proposed mechanism in contrast to an already existing one, which will be called non-redundant hereafter. Later presented gait simulations are solely performed with the VSM to demonstrate its practicability. The non-redundant design for an active ankle is shown in Figure 1 on the left, which has also been used e.g. in [17]. It comprises the actuation of two DOFs via two kinematic chains (2RRPS). A complete analytic solution of this ankle mechanism can be found in [16]. A representation of the proposed mechanism under study in this paper can be seen in Figure 1 on the right and depicts three kinematic chains attached to the fixed $\{s\}$ -frame and moveable $\{b\}$ -frame. In each chain, non-linear springs are attached in series to the actuators. In Section II and III the fundamental equations for modelling a 2-DOF flexible-redundant ankle joint and its stiffness behaviour are derived. Derivations of the kinematic equations of the non-redundant ankle design are incorporated - neglecting springs and overactuation - that serve for a comparative study under Section IV-A. For this kind of analysis, it is sufficient to use pure kinematic relations (Equation 3). Subsequently, a simple demonstration of the mechanism behaviour is given in Section IV-B, followed by a human gait simulation in Section IV-C.

II. KINETOSTATIC MODEL

The flexible-redundant mechanism under study has spring elements which makes it inherently flexible and hence, does not allow a pure kinematic input - output relation. Rather, the input - output relations are deduced from a quasi-static equilibrium. For the flexible-redundant mechanism, the relevant coordinates are separated into *actuation space* $\mathbf{q}^a = (d_1^a, d_2^a, d_3^a)^T$ and *work space* $\mathbf{x} = (\rho, \nu)^T$. The variables of the compliant springs are denoted as $\mathbf{q}^f = (d_1^f, d_2^f, d_3^f)^T$ (see Figure 1). The generalized coordinates of the mechanism are $\mathbf{q} = (\mathbf{q}^a, \mathbf{q}^f)$. For the following discussion \mathbf{q}^f are considered passive coordinates, not affecting the structure of the Jacobian.

Table I presents the different quasi-static models that were derived in the scope of this paper in order to solve various

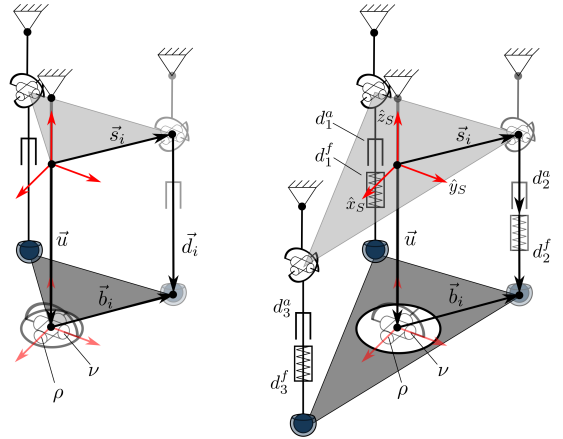


Fig. 1. Non-redundant and flexible-redundant ankle design with two end-effector DOFs (ρ : roll, ν : pitch). The DOFs are represented by a rotation of the $\{b\}$ -frame with respect to the $\{s\}$ -frame.

forward and inverse problems. We refer to *forward* models when actuator and spring deflection - the full set or a subset of generalized coordinates \mathbf{q} - is used as input. *Inverse* models make use of work space dependent quantities to obtain solutions for generalized coordinates \mathbf{q} . In Section IV-B a demonstration of model I in Table I takes place by computing the configuration of the mechanism from known actuator deflections. The simulations of human gait in Section IV-C are carried out with help of model III and IV and coherence is proved by a back computation by means of model II. In model III we make use of the end-effector force \mathbf{f} that is presented in this section, whereas the diagonal terms of the stiffness matrix $k_{\rho\rho}$ and $k_{\nu\nu}$ - used in model IV - are derived in Section III-B.

TABLE I
OVERVIEW OF THE DIFFERENT QUASI-STATIC MODELS - THE NUMBER OF OUTPUT VARIABLES ALSO DEFINES THE NUMBER OF NECESSARY EQUATIONS INSIDE EACH MODEL.

	Direction	Equations	Input	→	Output
I	forward	1, 5, 7	\mathbf{q}^a	3 → 5	\mathbf{x}, \mathbf{q}^f
II		1, 5, 7	$\mathbf{q}^a, \mathbf{q}^f$	6 → 4	\mathbf{x}, \mathbf{f}
III	inverse	1, 5, 7, $d_1^a = d_2^a$	\mathbf{x}, \mathbf{f}	4 → 6	$\mathbf{q}^a, \mathbf{q}^f$
IV		1, 9, $d_1^a = d_2^a$	$\mathbf{x}, k_{\rho\rho}, k_{\nu\nu}$	4 → 6	$\mathbf{q}^a, \mathbf{q}^f$

The geometric loop closure equations of the mechanism as represented by the distance constraints are given by

$$\|\vec{u} + \mathbf{R}^{sb}(\rho, \nu) \cdot \vec{b}_i - \vec{s}_i\| - (d_i^a + d_i^f) = 0 \quad \text{for } i = 1, 2, 3 \quad (1)$$

where the fixed offset between space frame $\{s\}$ and body frame $\{b\}$ is denoted by \vec{u} . Vectors \vec{s}_i are represented in the fixed $\{s\}$ -frame. On the contrary, \vec{b}_i are represented in the $\{b\}$ -frame and are therefore rotated by the rotation matrix $\mathbf{R}^{sb}(\rho, \nu) \in SO(3)$. Equation 1 is an explicit equation and

more generally, it can be considered a geometric equation of the form $\mathbf{g}(\mathbf{x}, \mathbf{q}^a, \mathbf{q}^f) = \mathbf{0}$. The corresponding velocity constraints are

$$\begin{aligned} \frac{\partial \mathbf{g}(\mathbf{x}, \mathbf{q}^a, \mathbf{q}^f)}{\partial \mathbf{q}^a} \dot{\mathbf{q}}^a &= - \frac{\partial \mathbf{g}(\mathbf{x}, \mathbf{q}^a, \mathbf{q}^f)}{\partial \mathbf{x}} \dot{\mathbf{x}} \\ \mathbf{J}_a(\mathbf{q}^a, \mathbf{q}^f) \dot{\mathbf{q}}^a &= -\mathbf{J}_x(\mathbf{x}) \dot{\mathbf{x}} \end{aligned} \quad (2)$$

The partial differentiation of the mapping $\mathbf{g} : \mathbb{R}^3 \rightarrow \mathbb{R}^2$ with respect to the actuator variables and work space variables leads to the Jacobian matrices $\mathbf{J}_a \in \mathbb{R}^{3 \times 3}$ and $\mathbf{J}_x \in \mathbb{R}^{3 \times 2}$ respectively. Equation 1 represents the constraints by a distance measure and generally appears as a square function. Since \mathbf{q} and \mathbf{x} do not form compositions or products in Equation 1, the left hand side of Equation 2 loses dependency on \mathbf{x} , while the right hand side loses dependency on \mathbf{q} due to partial differentiation. Thus, inverse and forward kinematics relations can be derived as

$$\begin{aligned} \dot{\mathbf{q}}^a &= -\mathbf{J}_a^{-1} \mathbf{J}_x \dot{\mathbf{x}} \\ &= \mathbf{J}(\mathbf{x}, \mathbf{q}^a, \mathbf{q}^f) \dot{\mathbf{x}} \\ \dot{\mathbf{x}} &= \mathbf{J}^\dagger(\mathbf{x}, \mathbf{q}^a, \mathbf{q}^f) \dot{\mathbf{q}}^a \end{aligned} \quad (3)$$

where $\mathbf{J} \in \mathbb{R}^{3 \times 2}$ is the kinematic Jacobian of the manipulator when considered as a rigid body system (provided \mathbf{q}^f) determined by the Jacobians \mathbf{J}_a and \mathbf{J}_x . To obtain Equation 3, an inversion of a non-square matrix becomes necessary. This inversion can be achieved by constructing the *Moore-Penrose pseudoinverse* according to [21] and indicated by a superscript \dagger . Pseudoinverse can be created numerically for instance by *Singular Value Decomposition (SVD)* as described by [13]. Same procedure applies for the non-redundant mechanism that serves for comparison in this study. The difference is that the matrices \mathbf{J}_a and \mathbf{J}_x are invertible, having input and output vector in Equation 3 of equal dimension.

The manipulator comprises of series-elastic actuators with non-linear springs in each leg. Thus, the actuator force is equal to the force in the flexible element (whose deflection is described by \mathbf{q}^f). A possible spring characteristic is derived in Section III-A. Hence, actuator forces $\boldsymbol{\tau}$ and end-effector forces $\mathbf{f} = (f_\rho, f_v)$ are related with the kinematic Jacobian matrix of the manipulator.

$$\boldsymbol{\tau} = \mathbf{J}^{\dagger T} \mathbf{f} \quad (4)$$

$$\mathbf{f} = \mathbf{J}^T \boldsymbol{\tau} \quad (5)$$

Consequently, the relation between the actuator coordinates and work space coordinates is determined by the end effector load and actuator forces.

Remark: Inverse models are always restricted to pure pitch movements, since solvability of the system is ensured by the condition $d_1^a = d_2^a$. Inverse models can be used to solve problems where “outer” loads are known.

III. STIFFNESS MODEL

To actively change stiffness of VIAs, the implementation of non-linear spring characteristics is indispensable, as it is

shown in [9]. Stiffness of a parallel mechanism depends on the end-effector pose, but to reach certain stiffness values it also relies on an introduced non-linearity of the compliant elements. To fulfill this requirement, a compact design has been opted and thus pneumatic springs are introduced in each actuation leg. The derivation of the spring characteristic is given subsequently in Section III-A. Altering the stiffness of the end-effector is one of the aims of this work and therefore a stiffness representation in work space for the ankle mechanism is derived in Section III-B. It allows to compute the 2D stiffness of the ankle for a given configuration.

A. Pneumatic Spring Model

In Figure 2 a double-acting pneumatic spring is shown for which a symmetric spring characteristic can be obtained around the zero position.

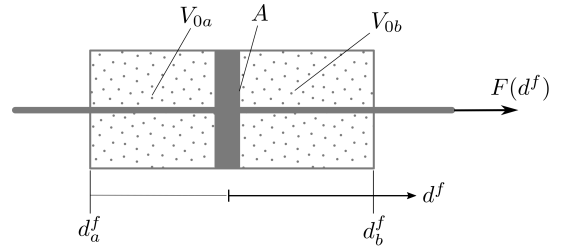


Fig. 2. Double enclosed pneumatic cylinder with the piston area A and the position dependent force $F(d^f)$. With the strokes d_a^f and d_b^f , the volumes V_{0a} and V_{0b} are formed (under neglect of the pistons height).

Assuming an adiabatic and reversible compression/depression of the cylinders, it is allowed to use the isentropic relation for pressure changes

$$\frac{p_1}{p_0} = \left(\frac{V_0}{V_1} \right)^\kappa \quad (6)$$

Equation 6 gives a pressure ratio between state (1) and (2) expressed by a volume ratio with κ as the heat-capacity ratio. When supposing that the initial pressure and volume is equal on both sides of the piston, a force expression can be given with help of Equation 6, so that

$$F(d^f) = c_0 \cdot \left[\frac{1}{(d_0^f + d^f)^\kappa} - \frac{1}{(d_0^f - d^f)^\kappa} \right] \quad (7)$$

where d_0^f is the maximal piston stroke and $c_0 = p_0 A \cdot (d_0^f)^\kappa$ the *pneumatic constant*. The required non-linearity of the spring elements is fulfilled by introduction of Equation 7 in the system. A plot of the force and energy function can be seen in Figure 3, indicating also that the force is almost linear over a range of approximately 20% piston stroke. Active stiffness changes can thus be achieved where the underlying derivations are carried out in the subsequent section.

B. Stiffness Representation in Work Space

As stiffness is defined by the ratio of infinitesimal force change and position change, an expression for the end-

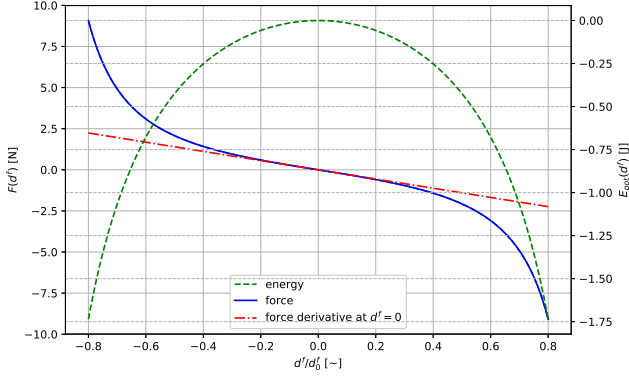


Fig. 3. Pneumatic spring force $F(d^f)$ and potential energy $E_{pot}(d^f)$ stored in the spring for a unit pneumatic constant ($c_0 = 1$) over normalized piston stroke d^f/d_0^f .

effector according to [26] can be given by

$$\begin{aligned}
 \mathbf{K} &= \frac{\partial \mathbf{f}}{\partial \mathbf{x}} \\
 &= \frac{\partial (\mathbf{J}^{\dagger T} \boldsymbol{\tau})}{\partial \mathbf{x}} \\
 &= \mathbf{H}^T \boldsymbol{\tau} + \mathbf{J}^{\dagger T} \frac{\partial \boldsymbol{\tau}}{\partial \mathbf{x}} \\
 &= \mathbf{H}^T \boldsymbol{\tau} + \mathbf{J}^{\dagger T} \frac{\partial \boldsymbol{\tau}}{\partial \mathbf{q}^a} \mathbf{J}^{\dagger} \quad (8)
 \end{aligned}$$

with \mathbf{H}^T being the $2 \times 3 \times 2$ transpose of the Hessian matrix¹ and $\partial \boldsymbol{\tau} / \partial \mathbf{q}^a$ being a diagonal matrix carrying the spring rates of the passive elements.

Because of the serial attachment of actuators and springs and assuming quasi-static configuration changes, the actuator forces $\boldsymbol{\tau}$ in Equation 8 can be replaced by the force expression of the passive springs (Equation 7) and will be denoted with $\boldsymbol{\tau}^f$ in the following. This step brings the advantage of reducing the necessary inputs of the equation on a position level. As the spring forces are then function of \mathbf{q}^f only and derived by the active coordinates \mathbf{q}^a , the dependency \mathbf{q}^f must be substituted with help of the inverse kinematics expression (Equation 1). The replacement of the (otherwise active) force terms and the use of the inverse kinematics to obtain a (passive) diagonal matrix $\partial \boldsymbol{\tau} / \partial \mathbf{q}^a$, is the important modification of this model, since it allows to compute an exclusively configuration dependent stiffness in work space.

¹The Hessian of a scalar field is a square matrix, defined by $\mathbf{H}_{i,j} = \frac{\partial^2 g}{\partial x_i \partial x_j}$, but becomes a third order tensor of shape $\mathbf{H}(\mathbf{g}) = [\mathbf{H}(g_1) \ \dots \ \mathbf{H}(g_m)]$ when the derived function is a *vector field* $\mathbf{g} : \mathbb{R}^n \rightarrow \mathbb{R}^m$.

Conclusively, it can be written

$$\begin{aligned}
 \mathbf{K}(\mathbf{x}, \mathbf{q}^a, \mathbf{q}^f) &= \mathbf{H}^T \boldsymbol{\tau}^f(\mathbf{x}, \mathbf{q}^a) + \mathbf{J}^{\dagger T} \frac{\partial \boldsymbol{\tau}^f(\mathbf{x}, \mathbf{q}^a)}{\partial \mathbf{q}^a} \mathbf{J}^{\dagger} \quad (9) \\
 &= \begin{bmatrix} k_{\rho\rho} & k_{\rho\nu} \\ k_{\nu\rho} & k_{\nu\nu} \end{bmatrix}
 \end{aligned}$$

with $\boldsymbol{\tau}^f(\mathbf{x}, \mathbf{q}^a)$ being the passive forces in the actuation legs. They only depend on the configuration of the end-effector and the position of the actuators in this form.

Remark: During stiffness computations, it was found that the substitution in $\boldsymbol{\tau}^f$ of \mathbf{q}^f by \mathbf{q}^a in the first term of Equation 9 introduced high numerical errors in some configurations (especially for small d_0^f). We therefore recommend to keep the dependency on spring coordinates for $\boldsymbol{\tau}^f$ in the active stiffness term.

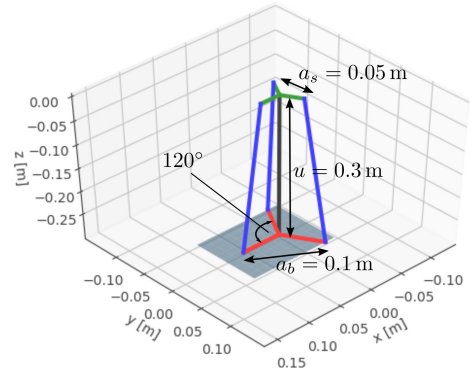


Fig. 4. Line plot depiction of the ankle geometry. The blue lines indicate the actuation legs that bear actuators and springs. Their attachment points in the $\{s\}$ - and $\{b\}$ -plane form equilateral triangles of edge length a_s and a_b . The attachment point of the front actuator is located on the roll axis.

IV. RESULTS & DISCUSSION

This section starts with a singularity and dexterity analysis of the mechanism by comparing the non-redundant system (Figure 1 left) and the flexible-redundant system (Figure 1 right). In the subsequent Section IV-B, the stiffness curves of exemplary computations with a forward quasi-static model are discussed. A comparison of the solutions to the free software *OpenModelica* can be found in [27] and is not presented here. We conclude this section with a simulation of the stance phase during walking in humans in Section IV-C, providing also a deeper discussion on the stiffness. All models treated in Section IV-B and IV-C are numerically solved by a *least squares method*. Geometric depiction of the mechanism is given in Figure 4 and is related to the design in [16].

A. Singularity and Dexterity in Work Space

In this section, we compare the non-redundant and flexible-redundant design, showing advantages of the flexible-redundant design in terms of singularity and dexterity. According to [20] and [26], the criteria coming from

vanishing determinant ($\det(\mathbf{J}\mathbf{J}^T) = 0$) and condition number ($\text{cond}(\mathbf{J}\mathbf{J}^T)$) can be used to assess singularity points and dexterity of the mechanism for the whole work space. The analysis is independent of the spring deflections \mathbf{q}^f and can therefore be used as a general statement on singularities and dexterity. Figure 5 on the left shows that singularities are completely removed from the work space and a depiction of low dexterity is given in the plot of the flexible-redundant design. Moreover, the plots in Figure 5 on the right indicate better dexterity of the flexible-redundant design around the zero pose. This behaviour is especially advantageous for an ankle joint.

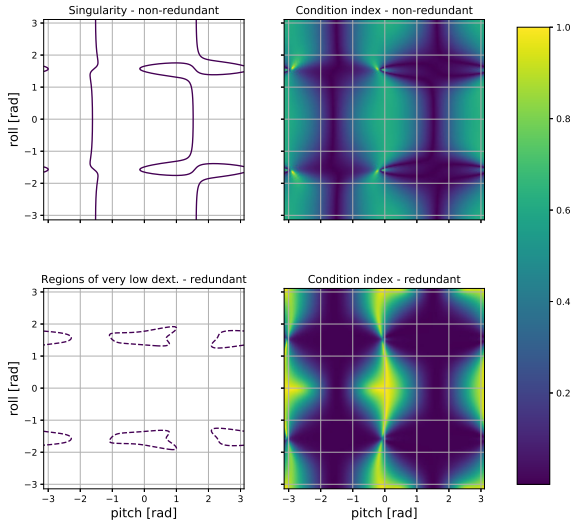


Fig. 5. Singularity curve (left) and dexterity plots (right) for the non-redundant and flexible-redundant design. Condition index is defined by $1/\text{cond}(\mathbf{J}\mathbf{J}^T)$ as normalized dexterity measure. The region of low dexterity incorporates values where $\det(\mathbf{J}\mathbf{J}^T)$ is in the interval $[10^{-6}, 2 \cdot 10^{-4}]$

B. Forward Kinetostatic Simulations

With the given geometry shown in Figure 4 and selected values for the pneumatic spring elements, kinetostatic simulations of forward type can be performed to gain insight about the behaviour of the mechanism. The pneumatic springs are defined with $A = \pi/4 \cdot 0.03^2 \text{ m}^2$, $p_0 = 1013.25 \text{ hPa}$, $\kappa = 1.4$ and $d_0^f = 0.15$, specified in Equation 7 inside the quasi-static model. Actuator lengths are changed in the range from $\pm 30\%$ of their initial length to alter the system. Variantly, one, two or three actuators are moved, while the other actuators are kept in their zero position. Results arising from the quasi-static model I are plotted in Figure 6 and are complemented by the *eigenvalues*² of the stiffness matrix - denoted by k_ρ and k_v - (Equation 9) to account for stiffness in roll and pitch direction.

²Taking the eigenvalues of \mathbf{K} allows to retrieve the stiffness felt by applying deflections in the main directions of the ankle also for mixed load cases.

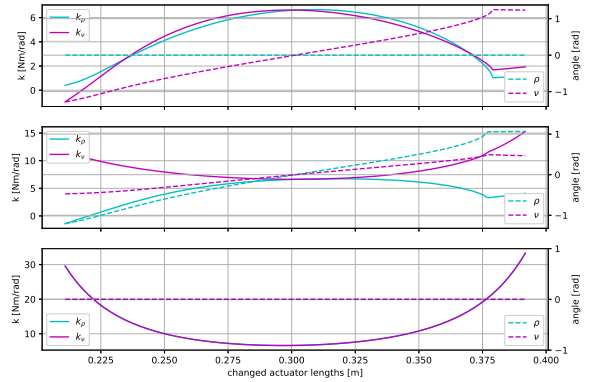


Fig. 6. Stiffness and position curves in work space of the mechanism for three load cases, when selected actuators are moved $\pm 30\%$ of their initial length. **Upper plot:** Only the front actuator d_1^q , lying on the roll axis is moved. **Center plot:** Front actuator d_1^q and one rear actuator d_2^q are moved simultaneously. **Lower plot:** All three actuators are moved simultaneously.

C. Human Gait

The biomechanical data from human stance phase [11] is utilized for the assessment of the mechanism. Human gait is dynamic, but in the scope of this paper we are interested in the general feasibility of the mechanism and use therefore simpler quasi-static models. By giving input to the inverse model III (see Section II) by means of biomedical gait data (Figure 7), it was assessed whether the mechanism can adapt to this preset position and torque that occur in human ankles. Movement and loads only occur in pitch and thus $v = f_v = 0$. During simulation, it was found that the piston stroke of the pneumatic springs must be decreased in order to find solutions to the problem and thus a value of $d_0^f = 0.015 \text{ m}$ was chosen for gait simulations. Furthermore, the solver³ requires bounds on all spring coordinates d_i^f what has been set to 99.9% of d_0^f .

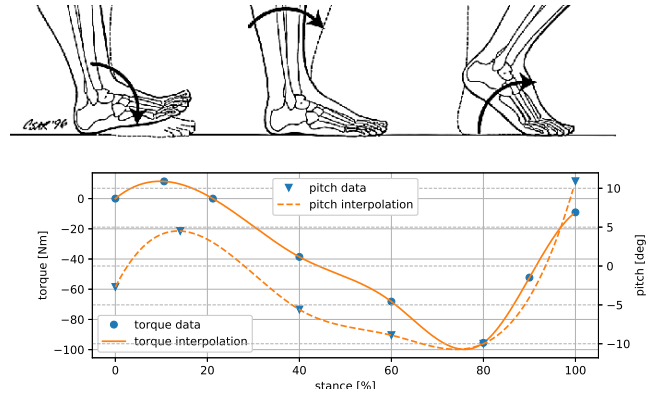


Fig. 7. Biomedical data of pitch torque and pitch angle over stance as input to the inverse quasi-static model III. Single data points are retrieved from [11] (blue points) and are interpolated by cubic splines. Foot depiction from [1]

³Here, the package `scipy.optimize.least_square` in the *Python* language was used.

Upper and centre plot in Figure 8 show the solution output of model III in the configuration space, arising from the biomedical input in work space (in Figure 7). According to the pure pitch movement of the mechanism, the rear actuators (d_1^a, d_2^a) and springs (d_1^f, d_2^f) possess the same solution curves. Complementary, stiffness in roll and pitch direction are depicted in the lower plot of the figure, showing considerable stiffness increase in the mechanism during gait with maximal values at around 75% of stance. This is mainly due to increasing input torque in this region leading to higher spring forces and thus higher stiffness. A back-computation by means of the forward model II showed consistency between model II and III by recomputing \mathbf{x} and \mathbf{f} as given in Figure 7.

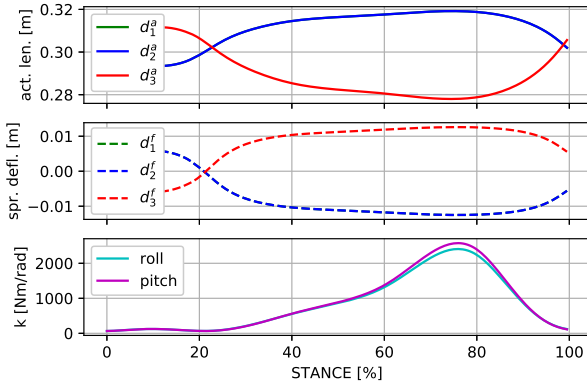


Fig. 8. Non-unique solution of the inverse model III with input values for pitch angle and torque given by Figure 7.

Model III does not deliver a unique solution, since internal forces can be generated inside the mechanism that do not affect the pose and torque of the end-effector. We can also specify the end-effector pose \mathbf{x} (biomedical data) and define some stiffness in advance to solve for the configuration of the mechanism what refers to inverse model IV. This is only possible for the here given *symmetric* case of pure pitch, where the stiffness is fully represented by the diagonal terms of \mathbf{K} . The stiffness values from the previous gait simulation have been taken and augmented by a factor of 1.5 to compute the configuration of the mechanism shown in the upper and centre plots of Figure 9. In this specific case, \mathbf{x} and (k_{pp}, k_{vv}) serve as input and as expected, the end-effector force \mathbf{f} resulting from the computation does not follow the torque depicted in Figure 7.

By successfully computing the configuration \mathbf{q} of the mechanism by means of biomedical data (combined position and force data - \mathbf{x} and \mathbf{f}), it has been shown that the general idea of the mechanism is feasible e.g. for an ankle design. Besides, it has been demonstrated that stiffness can also serve as input to the mechanism. The non-uniqueness of the solutions in configuration space leaves freedom for further parameter control, such as for energy. This raises the idea of stiffness control for the whole mechanism while making use

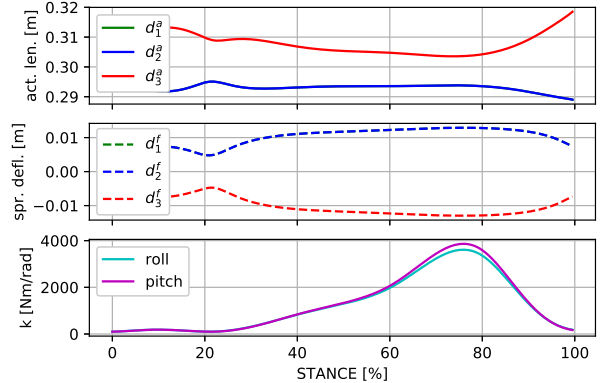


Fig. 9. Solution for the stance phase when stiffness values and pitch movement serve as input to the system - model IV. Stiffness values coming from Figure 8 are increased by a factor of 1.5 and serve as input in the underlying computation.

of its compliance, what might be very advantageous e.g. for semi-passive walkers and pointing towards energy-optimized mechanisms.

V. CONCLUSION

The idea of a VSM, that is a combination of RPM and VIA, was proposed and defined in this paper. As one major idea of this mechanism is to change the stiffness of this multi-DOF mechanism, an adapted stiffness formulation was derived besides its kinematic description. Comparison with a non-redundant mechanism showed an improvement in terms of singularity avoidance and increased dexterity. Using quasi-static formulations, different load cases for the ankle VSM were computed. Biomechanical data of the stance phase during human gait were fed to the system, showing that movements can be adapted under different stiffness characteristics of the end-effector. In contrast, predefined stiffness was also assessed as input data, raising the possibility of adaptable energy optimization e.g. for walkers.

ACKNOWLEDGMENT

The work presented in this paper was performed within the project TRANSFIT, funded by the German Aerospace Center (DLR) with federal funds from the Federal Ministry for Economic Affairs and Energy (BMWi) (Grant Nos. 50RA1701, 50RA1702 and 50RA1703). The fifth author acknowledges the support from the LCM K2 Center for Symbiotic Mechatronics within the framework of the Austrian COMET-K2 program.

REFERENCES

- [1] Z.O. Abu-Faraj, G.F. Harris, P.A. Smith, and S. Hasani. *Wiley Encyclopedia of Electrical and Electronics Engineering*. John Wiley & Sons, 2015.
- [2] B. Vanderborght et al. "Variable impedance actuators: A review". In: *Robotics and Autonomous Systems* 61 (2013), pp. 1601–1614.

- [3] A. Albu-Schäffer et al. “Soft Robotics - Adaptable Compliance”. In: *IEEE Robotics & Automation Magazine* (2008), pp. 20–30.
- [4] D. Chakarov. “Study of the antagonistic stiffness of parallel manipulators with actuation redundancy”. In: *Mechanism and Machine Theory* 39 (2004), pp. 583–601.
- [5] A. Dietrich, T. Wimböck, and A. Albu-Schäffer. “Dynamic Whole-Body Mobile Manipulation with a Torque Controlled Humanoid Robot via Impedance Control Laws”. In: *Proc. IEEE Int. Conf. on Intelligent Robots and Systems* (2011), pp. 3199–3206.
- [6] E.D. Fasse and J.F. Broenink. “A Spatial Impedance Controller for Robotic Manipulation”. In: *Proc. IEEE Transactions on Robotics and Automation* 13 (1997), pp. 546–556.
- [7] C. Gosselin and J. Angeles. “Singularity Analysis of Closed-Loop Kinematic Chains”. In: *IEEE Transaction on Robotics and Automation* 6 (1990), pp. 281–290.
- [8] S. Haddadin et al. “Intrinsically Elastic Robots: the Key to Human Like Performance”. In: *IEEE/RSJ International Conference on Intelligent Robots and Systems* (2012), pp. 4270–4271.
- [9] R. Van Ham, T.G. Sugar, B. Vanderborght, K.W. Hollander, and D. Lefeber. “Compliant Actuator Designs”. In: *IEEE Robotics & Automation Magazine* - (2009), pp. 81–94.
- [10] N. Hogan. *Impedance Control: An Approach to Manipulation: Part III - Applications*. Massachusetts Institute of Technology, Cambridge. -. 1985.
- [11] M. Hora, L. Soumar, H. Pontzer, and V. Sladek. “Body size and lower limb posture during walking in humans”. In: *Exp Brain Res* 114 (1997), pp. 71–85.
- [12] A.G. Leal Junior, R. Milanezi de Andrade, and A.B. Filho. “Series Elastic Actuator: Design, Analysis and Comparison”. In: *INTECH Recent Advances in Robotic Systems* (2016), pp. 204–234.
- [13] D. Kalman. *A Singularly Valuable Decomposition: The SVD of a Matrix*. The American University Washington, DC 20016. 2002.
- [14] Elsa Andrea Kirchner, Niels Will, Marc Simnofske, and et. al. “Recupera-Reha: Exoskeleton Technology with Integrated Biosignal Analysis for Sensorimotor Rehabilitation”. In: *Transdisziplinäre Konferenz SmartASSIST*. 2016, pp. 504–517.
- [15] Shivesh Kumar, Bertold Bongardt, Marc Simnofske, and Frank Kirchner. “Design and Kinematic Analysis of the Novel Almost Spherical Parallel Mechanism Active Ankle”. In: *Journal of Intelligent & Robotic Systems* (2018). URL: <https://doi.org/10.1007/s10846-018-0792-x>.
- [16] Shivesh Kumar et al. “Kinematic Analysis of a Novel Parallel 2SPRR+1U Ankle Mechanism in Humanoid Robot”. In: *Advances in Robot Kinematics 2018*. Ed. by Jadran Lenarcic and Vincenzo Parenti-Castelli. Cham: Springer International Publishing, 2019, pp. 431–439.
- [17] S. Lohmeier, T. Buschmann, M. Schwienbacher, H. Ulbrich, and F. Pfeiffer. “Leg Design for a Humanoid Walking Robot”. In: *IEEE Humanoids* (2006), pp. 758–765.
- [18] S. Lohmeier, T. Buschmann, H. Ulbrich, and F. Pfeiffer. “Modular joint design for performance enhanced humanoid robot LOLA”. In: *Proceedings 2006 IEEE International Conference on Robotics and Automation, 2006. ICRA 2006*. 2006, pp. 88–93.
- [19] M. Luces, J.K. Mills, and B. Benhabib. “A Review of Redundant Parallel Kinematic Mechanisms”. In: *Journal on Intelligent Robotic Systems* 198 (2017), pp. 86–175.
- [20] J.-P. Merlet. “Jacobian, manipulability, condition number, and accuracy of parallel robots”. In: *ASME J Mech Des* (2006), pp. 199–206.
- [21] R. Penrose. “A generalized inverse for matrices”. In: *Mathematical Proceedings of the Cambridge Philosophical Society* 51 (1955), pp. 406–413.
- [22] F. Petit and A. Albu-Schäffer. “Cartesian Impedance Control For A Variable Stiffness Robot Arm”. In: *Proc. IEEE Int. Conf. on Intelligent Robots and Systems* (2012), pp. 4270–4271.
- [23] F. Pierrot, C. Reynaud, and A. Fournier. “DELTA: a simple and efficient parallel robot”. In: *Robotica* 8 (1990), pp. 105–109.
- [24] N.A. Radford, P. Strawser, K. Hambuchen, and et. al. “Valkyrie: NASA’s First Bipedal Humanoid Robot”. In: *Journal of Field Robotics* 32.3 (2015), pp. 397–419. URL: <http://dx.doi.org/10.1002/rob.21560>.
- [25] J.K. Salisbury. “ACTIVE STIFFNESS CONTROL OF A MANIPULATOR IN CARTESIAN COORDINATES”. In: *Proc. IEEE Conf. Decision Contr.* (1980), pp. 95–100.
- [26] S.Kock and W.Schumacher. “A Parallel x-y Manipulator with Actuation Redundancy for High-Speed and Active-Stiffness Applications”. In: *International Conference on Robotics & Automation* (1998), pp. 283–292.
- [27] C. Stoeffler. “Conceptual Design of a Variable Stiffness Mechanism using Parallel Redundant Actuation”. MA thesis. Belgium: University of Liège - Faculty of Applied Science, 2018.
- [28] S. Wolf and A. Albu-Schäffer. “Towards a Robust Variable Stiffness Actuator”. In: *IEEE/RSJ International Conference on Intelligent Robots and Systems (IROS)* (2013), pp. 5410–5417.
- [29] S. Wolf and G. Hirzinger. “A New Variable Stiffness Design: Matching Requirements of the Next Robot Generation”. In: *IEEE International Conference on Robotics and Automation* (2008), pp. 1741–1746.